
AN EFFICIENT INSECT-INSPIRED APPROACH FOR VISUAL POINT-GOAL NAVIGATION

Lu Yihe

School of Informatics
University of Edinburgh
Edinburgh, Scotland
yihe.lu@ed.ac.uk

Barbara Webb

School of Informatics
University of Edinburgh
Edinburgh, Scotland
bwebb@ed.ac.uk

January 26, 2026

ABSTRACT

In this work we develop a novel insect-inspired agent for visual point-goal navigation. This combines abstracted models of two insect brain structures that have been implicated, respectively, in associative learning and path integration. We draw an analogy between the formal benchmark of the Habitat point-goal navigation task and the ability of insects to learn and refine visually guided paths around obstacles between a discovered food location and their nest. We demonstrate that the simple insect-inspired agent exhibits performance comparable to recent SOTA models at many orders of magnitude less computational cost. Testing in a more realistic simulated environment shows the approach is robust to perturbations.

Keywords Point-goal Navigation · Habitat · iGibson · Insect-inspired AI Robot · Central Complex · Mushroom Body · Online Learning · Memory Consolidation

1 Introduction

Goal-directed navigation requires an intelligent agent, artificial or biological, to reach a goal through motion planning and control. It has wide real-world applications in mobile robots, from indoor to outdoor, spanning ground, underground, marine, and aerial scenarios. One of its particular forms, *point-goal navigation*, has recently been standardised and popularised by the annual Habitat navigation challenges ‘to benchmark and accelerate progress in embodied Artificial Intelligence (AI)’ [1]. At the start of point-goal navigation, the agent is provided with the explicit position (two-dimensional coordinates) of the goal (a point with a small catchment area) and tasked to reach it without an a priori map. In an obstacle-free environment, point-goal navigation can be solved by Path Integration (PI), i.e., dead reckoning, solely. In a more complex environment, however, the agent must employ other techniques to perceive obstacles (or traversable space) and take appropriate, ideally predictive, actions to find and follow an efficient path towards the goal. Typically, the Habitat point-goal navigation task considers an agent relying primarily on vision from a front-facing camera mounted on a robot.

Two contrasting solutions have been widely adopted over the years. A traditional approach is to create, update, and utilise a map on the fly, i.e., perform visual *Simultaneous Localisation And Mapping (SLAM)*. As the map grows in size and fidelity, motion planning becomes less error-prone. More recently, *Reinforcement Learning (RL)* approaches have increased in popularity, often making the assumption that there is no need for an explicit map. In particular, an End-to-end RL agent is expected to learn the direct correspondence between sensory inputs and (desired) control outputs, using general-purpose RL methods. Notably, the State-Of-The-Art (SOTA) agent, reported to achieve *perfect* performance in the Habitat point-goal navigation task [2], was obtained by RL. More specifically, [3] developed a near-perfect agent by massively scaling up Proximal Policy Optimisation (PPO), the de facto standard method of deep RL, into Decentralised Distributed PPO (DDPPO), and later [2] obtained the perfect agent with the same DDPPO method but using a larger and more accurately curated dataset of virtual scenes.

Here we adopt a third approach by considering a direct parallel to point-goal navigation observed in the behaviour of insects, such as ants, attempting to return to their nest after foraging. Many insects are able to maintain, through PI, an estimate of their position relative to the nest over long journeys away from it, and will attempt to return on a straight line towards it when food is located [4]. Moreover, during this return, the insect acquires visual information [5] that improves its efficiency in negotiating obstacles [6], leading to faster returns along improved paths on subsequent trips [7]. Recent neuroethological and modelling studies have established plausible accounts of the neural circuits supporting these capabilities in insects, with a focus on two brain structures that are conserved and anatomically stereotypical across insect species. In particular, the *Mushroom Body (MB)* is specialised in associative learning [8, 9] and novelty (familiarity) detection [10], and the *Central compleX (CX)* in PI and motion planning [11] (see [12] for a recent review).

Over the last decade, the CX has been clearly established as the ‘compass’ circuit in the insect brain, combining multi-modal sensory inputs and self motion to maintain an estimate of heading direction with respect to an external reference frame and to control steering towards an internally specified goal direction [13]. A minimal augmentation of this circuit provides a basis by which an insect could integrate its velocity over a foraging journey [11], i.e., perform PI to estimate its own location and use this to move towards any location specified in the same reference coordinates [14]. Models of this circuit have shown its efficacy for such point-goal navigation [15, 16, 17, 18], including real-world tests on a aerial robot [19]. However, this work has either neglected obstacles or added simple obstacle avoidance mechanisms to negotiate obstacles that prevent direct movement towards the goal [20, 21].

The insect’s ability to memorise and follow visually familiar routes has been independently explained as deploying a ‘visual compass’, which operates in a fundamentally different way. As first proposed by [22, 20], this involves memorisation of multiple panoramic views and the use of template matching [23] to estimate view familiarity/novelty and thus align to the route direction. [24] explicitly identified a neural circuit known as the MB as a plausible substrate for this memory in the insect brain. In addition to follow-up works on route following [25, 26, 27], the same idea of the MB being a learnable visual compass is also applied to or corroborated by works on visual homing, similar to point-goal navigation but the agent can rely only on vision (no odometry) in testing and the same scene is used in training and in testing [28].

In some of these MB models, route following has been combined with (non-visual) obstacle avoidance to improve robustness. An agent can be first guided along a route once and thus implicitly learns a route that avoids obstacles (the ‘teach and repeat’ task in robot navigation) [27]. Or, an agent can perform visual route learning during its initial homing attempt that does not rely on vision, but guided by PI and obstacle avoidance [20]. Although this implementation combines the functions of CX and MB, there is a hard switch from the first traversal (using CX for homing and MB for visual learning) to subsequent traversals (using MB only for visual route following). Recently, several existing models explore more organic integration of CX and MB circuits, demonstrating emergent behaviours of such agents, e.g., automatic switch from PI to visual homing when displaced to an arbitrary position, maintaining goal approaching locomotion when target object is temporarily obscured or removed [16, 17]. However, all these models have an initial training phase and, consequently, do not address how a ‘correct’ route is formed in the first place. This question was more thoroughly studied in [29, 30, 31, 7]. In particular, [31] explicitly demonstrated ‘ants learn *continuously* the routes ... in one trial’ by behavioural experiments and emulated the continuous learning and navigating of ants with the first-ever computational (non-neural) model with no prior training.

Here, we aim to develop an integrated model of these two insect navigation circuits (CX and MB) and assess the performance in realistic indoor robotic point-goal navigation simulations. In brief, the CX is responsible for determining control signals based on desired (goal-directed) and actual orientations, while the MB learns the association between visual inputs and collisions and uses the learnt association to modulate the CX computation. We hypothesise that, starting with zero prior memory, our model can gradually learn to avoid obstacles in a predictive manner, improving its route towards a goal even on the first trial, but increasingly so after repetition, which may even lead to a successful trial after failures. We first test our model in the Habitat simulator [1] (offering the standardised point-goal navigation task of the 2019 Habitat Challenge), permitting direct performance comparison between our model and others reported in recent literature. We then deploy our model in the iGibson simulator [32], which offers a more realistic physics engine than Habitat, to examine the contributions from the model components through ablation studies and the model’s robustness in steering by adding artificial noise and bias.

This paper is organised as follows: §2.1 introduces our insect-inspired model, §2.2 describes the experimental setup, §3 presents the main experiment results, and §4 discusses the implications.

2 Methods

2.1 Insect-inspired Model

Our insect-inspired model is primarily composed of two modules, the CX and the MB, emulating in simplified form the corresponding insect brain structures and their functions (Figure 1A). The CX generates control commands and performs PI using odometry inputs. By default, it chooses the direction towards the goal as the desired target direction. After a collision, the model tries to *escape* from the obstacle by the CX setting a temporary target different from the goal. In addition, the MB is triggered to *learn* visual inputs just before collisions and after escapes. Except during escapes, the MB modulates the target direction chosen by the CX based on visual memory, which is expected to reduce risks of future collisions by recognising visually similar obstacles.

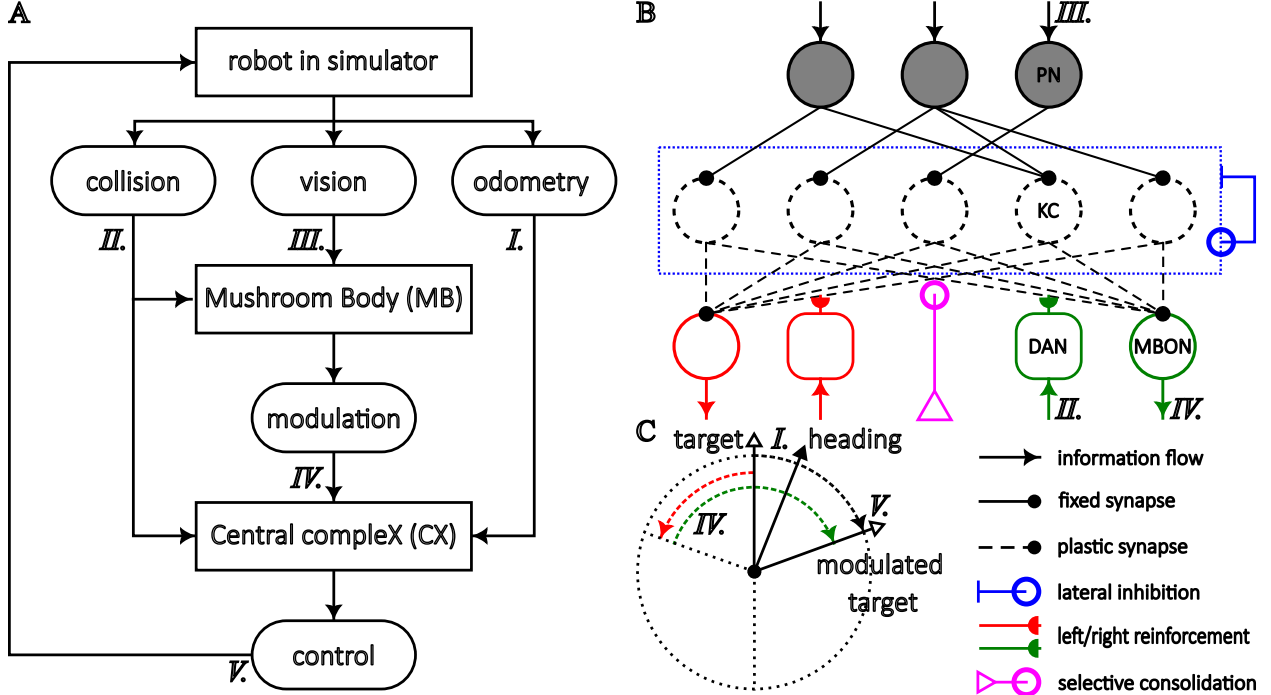


Figure 1: Overview of our insect-inspired model. (A) The closed-loop learning and control of our model embodied in a virtual robot. The model is primarily composed of two insect brain-like modules, a mushroom body (MB) and a central complex (CX). They use three types of (preprocessed) data as inputs, odometry (I), collision (II), and vision (III) to calculate a desired target direction, which determines control commands to be sent to the robot (V). (B) The MB architecture. The architecture is primarily feedforward, consisting of projection neurons (PNs), Kenyon cells (KCs), and left and right MB output neurons (MBONs); there is also lateral inhibition amongst the KCs. The activation of the PNs encode preprocessed visual information (I), and the activation of the MBONs is the modulatory signal projected from the MB to the CX (IV). The PN-KC synapses are predetermined with random initialisation, and the KC-MBON synapses are plastic. In particular, their plasticity is gated by dopaminergic neurons (DANs), receiving reinforcement signals determined by the urge to escape (II). An escape urge is produced after collision detection with a punishment signal that fades away after a fixed duration with a reward signal following. Recent changes of KC-MBON weights are consolidated into long-term memory, given improved task performance; otherwise, the changes are discarded. (C) The angular calculation performed by the CX. A target direction is set, either towards the goal or to escape an obstacle, and then modulated by the MB signals (IV) to the left or right side, based on which MBON is more activated. The modulated target is then compared to the current orientation (I) to calculate the desired rotation.

2.1.1 Visual Preprocessing

The raw images from the RGB camera of the robot are greyscaled, downsampled, and then processed by the Difference Of Gaussian (DOG) algorithm for feature (potentially edge) enhancement [33]. Such low-resolution vision is consistent

with insect compound eye optics [34, 35], and proved sufficient to produce good (or even better) performance while reducing computational costs [36, 37, 26, 27] (in particular, [37] employs the Sobel filter for edge detection).

2.1.2 Mushroom Body (MB)

The MB is an artificial neural network consisting of $N_{\text{PN}} = 1089$ Projection Neurons (PNs), $N_{\text{KC}} = 32000$ Kenyon Cells (KCs), 2 MB Output Neurons (MBONs), and 2 DopAminergic Neurons (DANs) (Figure 1B). Except for the lateral inhibition amongst the KCs, the MB architecture is primarily feedforward with the unidirectional connections from PNs to KCs to MBONs. More specifically, the PN activation encodes a preprocessed visual input, \mathbf{x} , which is transformed into a latent KC representation by

$$\mathbf{y}(t) = g_{\mathbf{W}_0}(\mathbf{x}(t)) = g(\mathbf{W}_0 \cdot \mathbf{x}(t)), \quad (1)$$

and subsequently the two MBON outputs are obtained by

$$\mathbf{z}(t) = \begin{bmatrix} z_L(t) \\ z_R(t) \end{bmatrix} = f_{\mathbf{W}_1}(\mathbf{y}(t)) = \frac{\mathbf{W}_1(t) \cdot \mathbf{y}(t)}{k}, \quad (2)$$

where $g(\cdot)$ is a k -Winners-Take-All (WTA) function with $k = 320$, making $\mathbf{y}(t)$ sparse and binary, \mathbf{W}_0 the PN-KC synaptic weight matrix, and $\mathbf{W}_1 = [\mathbf{W}_L, \mathbf{W}_R]$ the KC-MBON matrix. While \mathbf{W}_0 is predetermined by random initialisation to be binary and sparse, \mathbf{W}_1 is all-to-all and plastic (and thus dependent on t) with all the individual weights initialised at 1.

We highlight that \mathbf{W}_1 is the only plastic component within the MB and the entire model. In particular, learning of \mathbf{W}_L and \mathbf{W}_R is gated by the corresponding DANs, which encodes collision-related reinforcement in an all-or-none manner. If the left or right DAN is activated, it depresses the corresponding KC-MBON weights by

$$\Delta W_{ji}(t) = -\alpha \cdot y_i(t - \tau_e) \cdot W_{ji}(t - \tau_e), \quad (3)$$

where $\alpha \in (0, 1]$ is a user-defined learning rate, i the index of KC, $j \in \{\text{L}, \text{R}\}$, and $\tau_e \geq 0$ a user-defined time parameter. Note $\Delta W_{ji}(t) \in [0, 1]$ for any t , as $y_i \in \{0, 1\}$ and W_{ji} is initialised at 1, i.e., $\mathbf{W}_1(t=0) = \mathbf{1}$. More specifically, when the robot collides with an obstacle (receiving a punishment), on its left (or right) side, the left (or right) DAN will be activated to depress \mathbf{W}_L (or \mathbf{W}_R), in order to learn to avoid the same collision in future [38]. In addition, when the robot is released from its escape induced by the collision (omission of punishment is rewarding [39]), the opposite, right (or left) DAN will be activated, and \mathbf{W}_R (or \mathbf{W}_L) will be depressed accordingly.

Functionally, the MB architecture (with a single MBON) approximates a Bloom filter for novelty detection [40]. As \mathbf{W}_1 is updated only according to visual inputs just before collisions and after escapes, $z_L, z_R \in [0, 1]$ encode the left and right visual novelty, or effectively the perceived absence of obstacles on the two sides, respectively.

Furthermore, inspired from the different time scales of MB memory [41, 42], we assume

$$\Delta \mathbf{W}_1 = \mathbf{1} - \mathbf{W}_1 = \Delta \mathbf{W}_{\text{LTM}} + \Delta \mathbf{W}_{\text{ITM}} + \Delta \mathbf{W}_{\text{STM}}, \quad (4)$$

where the partition of Short-Term Memory (STM), Intermediate-Term Memory (ITM), and Long-Term Memory (LTM) is made according to the temporal hierarchy of the point-goal navigation task (§2.2). Specifically, as the model is tested throughout a series of trials, $\Delta \mathbf{W}_{\text{STM}}$ accumulates all weight changes within the current trial, and $\Delta \mathbf{W}_{\text{ITM}}$ the total change of the previous trial. At the end of the current trial, if the performance is improved (measured in Success weighted by Path Length, defined in §2.2.4), ITM is to be consolidated into LTM ($\Delta \mathbf{W}_{\text{LTM, new}} = \Delta \mathbf{W}_{\text{LTM, old}} + \Delta \mathbf{W}_{\text{ITM, new}}$). Whether consolidated or not, ITM is then overwritten by STM ($\Delta \mathbf{W}_{\text{ITM, new}} = \Delta \mathbf{W}_{\text{STM, old}}$), followed by the reset of STM ($\Delta \mathbf{W}_{\text{STM, new}} = \mathbf{0}$).

2.1.3 Central Complex (CX)

The CX is a module performing angular computations, primarily based on the robot's orientation, $\sigma(t)$, and the target direction, $\theta(t)$. In particular, the CX calculates the desired rotational angle as

$$\Delta \sigma(t) = \theta(t) - \sigma(t) + \phi(t), \quad (5)$$

where

$$\phi(t) = \pi \cdot (z_L(t) - z_R(t)), \quad (6)$$

denotes the MB modulation (Figure 1C). Note that $\phi(t) \in [-\pi, \pi]$ as $z_L, z_R \in [0, 1]$.

$\theta(t)$ is chosen to be the direction to the goal, $\theta^*(t)$, if no collisions have occurred recently. After colliding with an obstacle at $t = t_c$, a temporary target direction, $\theta'(t)$, is immediately set to the collision direction, $\gamma(t_c)$ (§2.2.2), and

Table 1: Robot specifications.

Simulator	iGibson	Habitat
Footprint Diameter	0.1677 m	0.2 m
Camera Height	0.0594 m	1.5 m
v_{\max}	2.133 m s^{-1}	$0.25 \text{ m frame}^{-1}$
ω_{\max}	$11.469 \text{ rad s}^{-1}$	$10^\circ \text{ frame}^{-1}$
FOV	$90^\circ \times 90^\circ$	$90^\circ \times 90^\circ$

gradually changes to the direction perpendicular to $\gamma(t_c)$ for $t \in [t_c, t_c + \tau_c]$, where t_c is the time of collision and τ_c the user-defined parameter of the model’s escape duration, effectively driving the robot away from the obstacle.

Starting without prior memory (\mathbf{W}_1 initialised to be all 1’s, implying $z_L = z_R$ and $\phi = 0$), the model attempts to drive the robot towards the goal in a straight line, until the robot collides with an obstacle. If the collision occurs on the left side, \mathbf{W}_L will be depressed. As a result, $z_L < z_R$ is expected in future when the robot is facing the same or a similar obstacle. Thus, the right side is more attractive (due to less anticipation of an obstacle), and consequently the MB modulation will promote a right turn.

2.2 Experiment Setup

Generally in point-goal navigation, an embodied model is expected to drive a robot from a starting position to a goal position using only its sensors, given no map (information of obstacles) but only the predetermined (two-dimensional) coordinates of the two positions. This work, in particular, considers agents with access to an RGB camera, accurate position and orientation (GPS+Compass) of the robot body, and collisions between the robot and any obstacles.

We tested our models in independent *episodes*, each composed of a sequence of *trials*. For any trial of the same episode, the scene, starting position and orientation, and goal position are identical. Throughout the trials of one episode, the MB of the insect-inspired model would keep learning, and consequently its modulation on the orientation would grow stronger until no collision occurs or the MB memory saturates. Across episodes, the MB memory was completely reset.

For extensive testing, in each of the two simulators (§2.2.1), the model underwent 100 episodes, each terminated after a trial in which LTM was not updated, or if the maximum trial number of 20 was reached. A trial would terminate after 500 frames or earlier if the goal was reached, i.e., a success (§2.2.4).

2.2.1 Simulation Platforms

We conducted our experiments in two simulators, Habitat [1] and iGibson [43, 32], with default settings. Both simulators offered realistic visual rendering, with the main limit on realism that the lighting is perfectly consistent. In both simulators, robots and other objects were perfect rigid bodies, and kinematics were deterministic (except when artificial noise was added). However, iGibson employed a realistic physics engine, simulating object motions based on the classical kinetics, whereas Habitat assumed significantly simplified kinematics, discretising robot motions completely, so that large-scale (RL) simulations could be performed more efficiently. In addition, objects other than the robot, e.g., chairs, were movable in iGibson but fixed in Habitat.

Our models were embodied in a primitive cylinder in Habitat and the Freight robot, scaled down from the default size by a factor of 0.3, in iGibson (see Table 1 for the specifications), both equipped with a front-facing RGB camera. Freight was chosen amongst the robots offered by iGibson, for its shape the most comparable to the cylindrical ‘robot’ in Habitat and its ability to reach the highest speeds, implying the longest possible distance of movement or a potentially minimal testing duration but a maximal difficulty for steering (due to inertia).

We used both simulators with virtual reconstructions of real-world indoor scenes in the Gibson dataset [44]. More specifically, Habitat was used with the 14 validation-split scenes from a larger set of high quality reconstructed scenes manually curated and rated by [1], known as Gibson 4+, and iGibson with its 15 default scenes.

2.2.2 Sensory Inputs

The FOVs of the front-facing RGB cameras on the two robots were identical (Table 1). Considering additionally that (at least part of) the same virtual reconstruction dataset were used, visual inputs in the two simulators would be similar in terms of generic visual features. A major difference was expected to be derived from the robots’ different heights. As the camera was placed at a lower height on Freight, visual inputs in iGibson always contained a larger portion of floor than in Habitat.

An RGB camera rather than an RGBD one was chosen, primarily because RGB cameras are more widely applicable. While the extra depth perception could always bring performance improvement (in simulations) [45, 1, 3, 46, 47, 2], the amount of such improvement is largely variable. All others equal, a depth-only model could outperform an RGB-only model [45, 2], and even an RGBD model [1]. Note our model could have used a monochrome camera for greater compatibility with insect vision and potentially enhanced efficiency in our model’s visual preprocessing (§2.1.1). However, RGB (or RGBD) vision is necessary for direct comparison with existing agents.

The odometry (position and orientation) data were extracted directly from the simulators and thus perfectly accurate (with the default settings). Although this assumption is unrealistic, insects can robustly estimate odometry and perform PI by sensory cue integration, primarily using the CX [12], and the assumption is consistent with other recent point-goal navigation work [45, 1, 3, 46, 47, 2].

The information of collision direction, γ , necessary for the model (§2.1.3), was not extracted directly from the simulators. In Habitat, after a collision event declared by the simulator, γ was approximated by the direction of the vector from the anticipated position (given the last action) to the actual position (due to sliding against the obstacle). In iGibson, a single force, \mathbf{F}_h , as the sum of all the external forces acting on the robot was projected onto the horizontal plane and compared to a predetermined threshold, F_c . If $|\mathbf{F}_h| \geq F_c$, a collision event was recorded with γ set to be the direction of \mathbf{F}_h .

2.2.3 Motion Control

Due to the drastic difference between the underlying physics of the two simulators, the permitted control signals were completely different. In Habitat, only one action, $a(t)$, at each frame, t , can be chosen out of the three options: move-forward (by 0.25 m), turn-left (rotation by 10°), and turn-right (rotation by -10°). Inertia and force (acceleration) were not considered. Given any control signal, the robot would change its position or orientation instantaneously within the frame. This change was perfect, unless a collision occurred, in which case the robot would slide against the obstacle with a displacement determined by geometry [1].

In contrast, the realistic physics engine of iGibson approximates continuous physics at a simulation frequency of 120 Hz, and the robot was controlled according to a pair of normalised linear and angular speeds, $v(t), \omega(t) \in [-1, 1]$, at the (default) visual rendering frequency of 30 Hz. The unnormalised speeds would then be obtained by multiplying v_{\max}, ω_{\max} (Table 1). Unlike in Habitat, however, these speeds as control signals could not be reached instantaneously, as the actuators were also physically realistic.

Consequently, after computing $\Delta\sigma(t)$ with Equation (5), the low-level motion control of the robots had to be different for the embodied model in these two simulators. In Habitat, $a(t)$ was set to be turn-left or turn-right if $|\Delta\sigma(t)| \geq 10^\circ$; otherwise, $a(t)$ was set to be move-forward. In iGibson, $(v(t), \omega(t)) = (\cos \Delta\sigma(t), -\sin \Delta\sigma(t))$.

For determinism, we further assumed that an embodied model could complete all necessary computations from sensory input processing to the above control signal generation within each frame.

2.2.4 Performance Metrics

We considered three metrics for measuring performance in the point-goal navigation task:

1. Success Rate (SR): whether the agent could reach the goal position with a catchment area of 0.2 m radius,
2. Success weighted by Path Length (SPL):

$$SPL = SR \cdot \frac{l}{\max(l, p)}, \quad (7)$$

where l denotes the geodesic distance, i.e., the length of the shortest path, between the start and the goal positions and p the length of the path taken by the robot under autonomous control,

3. Total number of collisions.

The first two metrics are widely reported in the recent literature of point-goal navigation, e.g., [45, 1, 3, 46, 47, 2]. The third metric was important for demonstrating that our model, which uses collision information (§2.1.3), could not just exploit passive sliding against obstacles as other models have been shown to do in these simulation environments [48].

Table 2: Seven recent point-goal navigation models. More details are summarised in Table 3 .

Model	Type	Camera	Training Epochs	SR	SPL	Reference
1	SLAM	RGB	5×10^6	0.090	0.047	Table 3 & 11 [45]
2		RGBD	7.5×10^7	0.62	0.51	Table 2 [1]
3	VO+RL	noisy RGB	1.47×10^7	0.79	0.61	Table 2 [46]
4		noisy RGBD	7.5×10^9	0.960	0.766	Table 1 [47]
5	End-to-end RL	RGB	7.5×10^7	0.64	0.46	Table 2 [1]
6		RGB	2.5×10^9	0.991	0.929	Table 2 [3]
7		RGB	1.5×10^9	1.00	0.90	Table 2 [2]

2.3 Model Comparison

2.3.1 SOTA Results

For benchmarking purpose, we identified seven notable models (amongst numerous variations) reported in six recent works on point-goal navigation [45, 1, 3, 46, 47, 2]). All the works tested their models in Habitat with the Gibson 4+ scenes [1], except [45] (published before the standarised Habitat challenge [1]), which used MINOS and Matterport3D scenes [49].

Their experiment setups are identical to ours (§2.2), except for three technical differences. Firstly, the standardised task does not provide agents with collision data (at least in testing), whereas our task does. Secondly, visual inputs are noisy in [46, 47], and their agents have access to odometry data only in training but not in testing. Thirdly, and most importantly, our experiment does not contain a separate training phase, as our model performs learning in testing on the fly. The provision of collision data does not give our model an edge in terms of information gain from sensory inputs, as it can be accurately inferred from odometry data in Habitat, and the ability to detect collisions is in any case a realistic assumption for robots and insects. Similarly, the absence of visual noise is not considered critical as our previous work on visual route following [27] has validated the visual robustness of a similar MB model in extensive simulations and the real world. We discuss further below the arbitrary and implicit role of odometry in previous experiments, again noting that the availability of approximate odometry is a reasonable assumption for robots and insects. As regards the third difference, to provide a fair comparison to the pre-trained models’ performances on new test scenes, we evaluate our model’s first attempt in a scene it has not experienced before.

The seven models we use for comparison can be classified into three types as listed in Table 2, based on their different assumptions of the spatial prior:

1. *SLAM* is designed to actively construct, maintain, and exploit a map. Empowered by the map, an agent can employ any local and global path planning techniques to find paths to the goal.
2. *Visual Odometry and RL (VO+RL)* asserts the efficacy of odometry. The greater modularity permits separate training of the two components and potential integration with other (non-visual) odometry sensors or estimation techniques.
3. *End-to-end RL* assumes no spatial prior. Using a trained policy, an agent selects actions based directly on sensory inputs.

All these models requires extensive training before testing. In particular, with billions of training frames, [3, 47] demonstrate two SOTA models of end-to-end RL and VO+RL, respectively, achieving near-perfect performance ($SPL \approx 1$) with RGBD inputs. Both models rely on the DDPPO algorithm, developed by [3], for large-scale, parallel training, and [2] sharpened the performance of the same DDPPO-based model to perfection ($SPL = 1$).

Note it was beyond the scope of our work to reproduce the SOTA results, and thus we copied the results directly from the cited works. We considered the best RGB models from each work, unless only the performance of the RGBD models is reported. According to all the works reporting both models, an RGBD model always outperforms the corresponding RGB model.

2.3.2 Ablation Studies

To examine the contributions of the three pathways, odometry (I), collision (II), and vision (III), of the insect-inspired model (Fig. 1A), we conducted ablation studies by removing firstly the vision pathway (producing the ‘odometry-collision model’) and subsequently the collision pathway (producing the ‘odometry-only model’, called ‘Goal-follower’ in [1, 45, 3]). Note that ablation of the collision pathway only would effectively disable the vision pathway, as the MB

learning had to be triggered by collisions, making the potential ‘odometry-vision model’ behaviourally equivalent to the odometry-only model. Further, the ablation of the odometry pathway would produce random exploration, similar to the ‘Random’ model reported in [1], which yielded performance as poor as $SR = 0.03$. Hence the odometry-only and odometry-collision models are the only relevant ablations to test.

3 Results

3.1 Goal Reaching with Minimal Learning

To highlight the efficacy and lightweightness of our insect-inspired model, we compare the average performance of the model’s first trials across 100 Habitat episodes (using STM only) with the results of the seven models in Table 2. While our model was outperformed by Models 4, 6, and 7, it achieved better or at least comparable performance to Models 1-3 and 5 (Fig. 2). Models 1-7 all required tens of millions of pre-training frames, whereas our model required no pre-training and used minimal online learning. Note all 500 frames of a single trial were considered to be training frames for the full model, as our model could learn in testing on the fly.

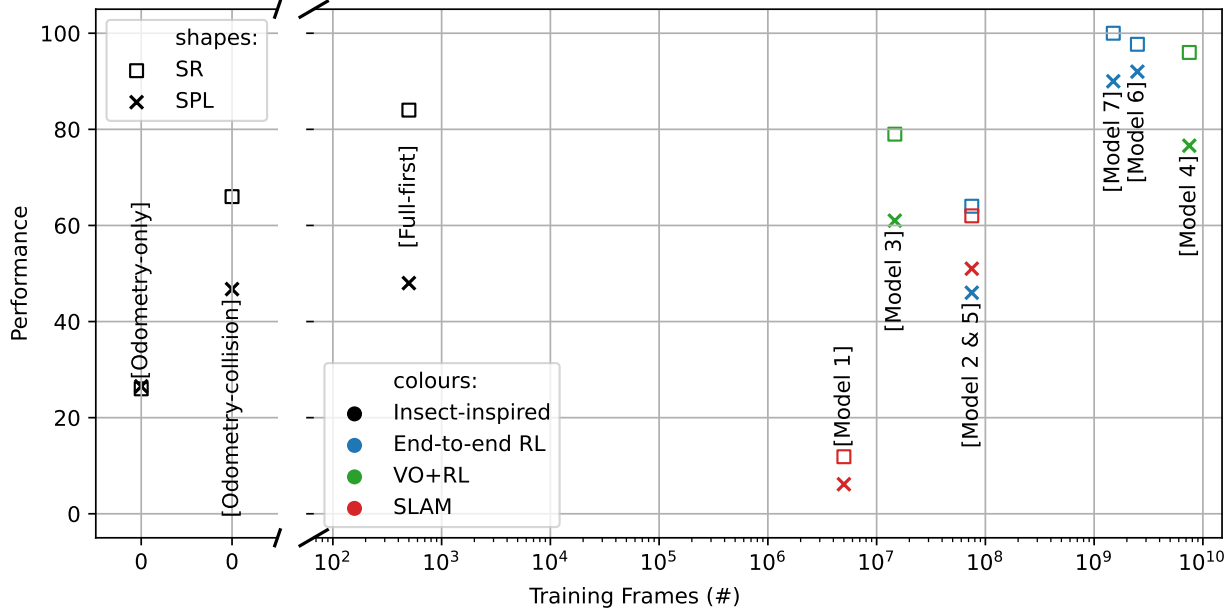


Figure 2: Model performance (SR (square) and SPL (cross), defined in §2.2.4) vs number of training frames. The results of our insect-inspired model (Full-first) and the ablated models (Odometry-only and Odometry-collision) were obtained from 100 independent test episodes in Habitat with the Gibson 4+ scenes by averaging the performance on the first trial for all test episodes. The tests were independent from each other with the full model’s memory reset each time. The results for the Models 1-7 are taken from the reported results summarised in Table 2. For fairer comparison, the performance of Model 1 is inflated deliberately by about a factor of 1.3 from that in Table 2, because [45] used a different simulator with a different dataset. The inflation factor is chosen based on the results in Table 2 of [1], where different results of the same model were reported for both Gibson and Matterport3D scenes.

Minimal learning was effective for our model to reach goals ($SR = 0.84$), because the model relied on the strong prior of goal approaching, and its learning was focused on mitigating the potential failures of the prior (i.e. avoiding obstacles). However, the prior helped the model little with choosing paths ($SPL = 0.48$), because the model’s (goal reaching) success was based on trial and error. It held absolutely no knowledge of the environment before its first attempt in each episode, and had to learn to move around obstacles from collisions on the fly. In contrast, when starting the testing, the RL and SLAM models would be able to visually recognise obstacles to some extent and could have even acquired some ‘common knowledge’ of floor plans from training scenes, potentially benefitting their (global) path planning in novel scenes.

Remarkably, despite its incapable of either seeing or learning, the performance of the ablated, odometry-collision model was comparable to that of Models 2 and 5. The substantial improvement over odometry only implies the importance of

the collision pathway for the robot not getting ‘stuck’ amongst obstacles. While learning in the full model improved the SR significantly, compared to odometry-collision, the improvement in SPL was negligible. Given the punitive definition of SPL based on SR, it can be inferred that, although the full model managed to solve many episodes that were failed for the ablated, odometry-collision model, its paths to the goals were far from optimal ($SPL \ll 1$).

3.2 Path Optimisation with Online Learning

While it was challenging for the insect-inspired model to find an optimal path to a goal at its first attempt, the model could potentially improve its performance in successive trials. To investigate whether and how the model optimises its path, we tested the model for up to 20 trials for every episode. The ablated models were still tested only once per episode, as they would merely repeat the trajectory (actually every movement) of the first trial in subsequent trials, due to their incapability of learning and the perfect determinism of the simulators.

In both simulators, the full model consistently outperformed the odometry-collision model on its first trial and achieved the best performance after a handful of trials of online learning (Fig. 3). For a subset of episodes, the odometry-collision model (incapable of learning) was unable to solve them ($SR = 0$). Thus, we also plot the results for the other models on these ‘hard’ episodes only, which reveals a stronger effect of learning over repeated trials for the full model (orange and red in Fig. 3).

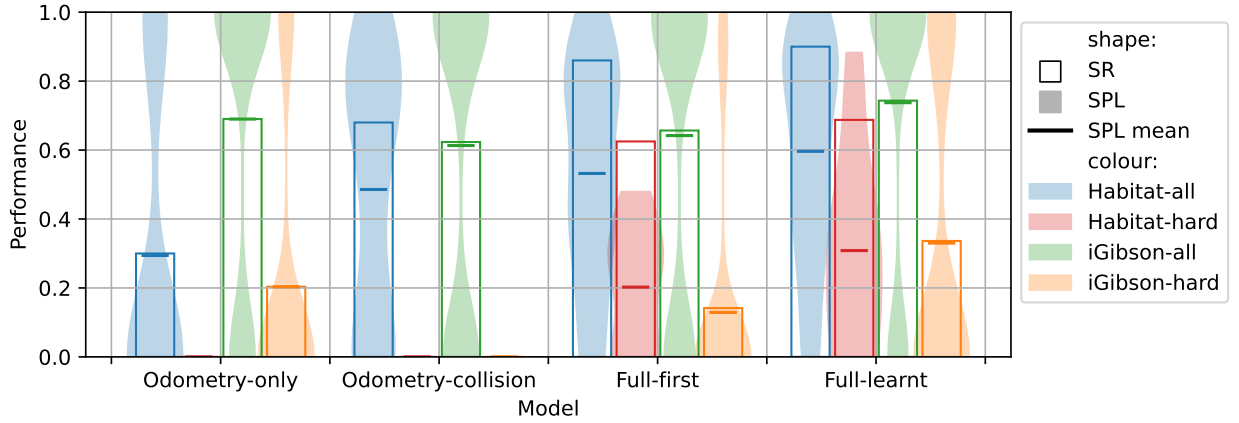


Figure 3: Performance of insect-inspired models in Habitat and iGibson. The odometry-only model has both vision and collision pathways ablated, and the odometry-collision model only the vision pathway ablated. Full-first and Full-learned represent the (same) full model’s performance at the first trials and when it completed learning. The episodes could not be solved by the odometry-collision model were considered ‘hard’, and thus the model scored 0.

Interestingly, the more ablated odometry-only model outperformed the odometry-collision model in iGibson, including solving some of the ‘hard’ episodes (Fig. 3). We note that this result was obtained only because the robot, as a perfect rigid body in the simulator, could keep sliding against obstacles without any physical damage. This allowed it to get past the obstacle but only at the expense of accruing a large number of collisions (Fig. 4), a circumstance generally unwanted in practice. In contrast, the collision pathway, relying on the simple reflexive escape mechanism, brought the number of collisions down by an order of magnitude, while learning reduced the collision risk further, as expected.

3.3 Memory Consolidation Prevented Performance Drop

With excessive memory consolidation, that is, if the model were to consolidate all ITM into LTM unconditionally without selection, the model, named full-excessive, would have yielded worse performance on average (Fig. 5). As the MB has a finite memory capacity (see [24, 27] for the theoretical estimation), the model grows more susceptible to memory interference that mistakenly anticipates the presence of an obstacle while facing traversable space after experiencing more collisions and learning more views. Consequently, the model became over-cautious and more likely to become trapped in a cluttered area or diverted towards a significantly wrong direction.

While selective consolidation of ITM into LTM avoided performance drop, it eliminated the possibility that the SPL could rebound after decrease, i.e., the performance might get stuck in a local minima. Indeed, we could construct a hypothetical agent that achieved a higher performance. Specifically, it saved all data of weight updates and the SPL at the end of every trial as checkpoints and could choose for each episode the checkpoint with the best performance

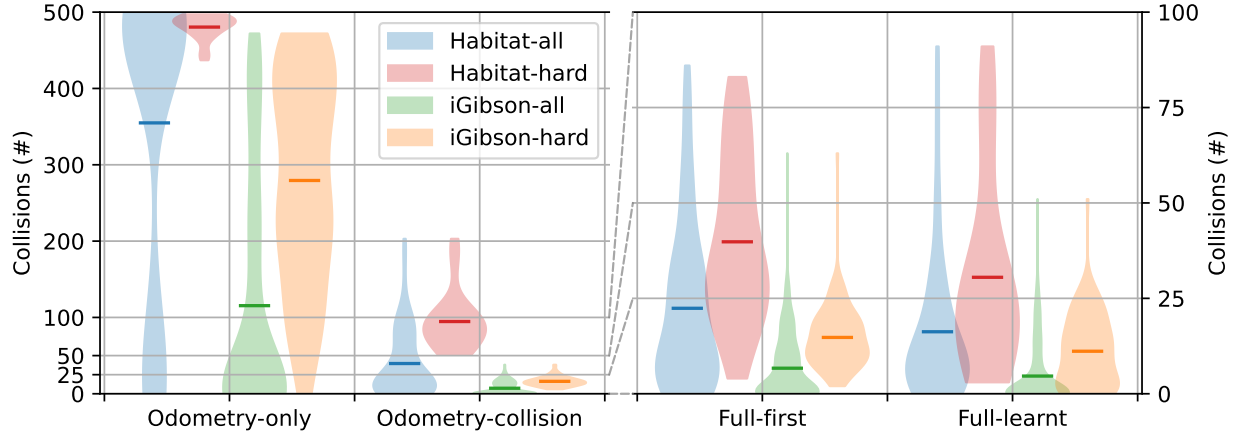


Figure 4: Summary of model collisions. Note the scales are different for the ablated vs full models.

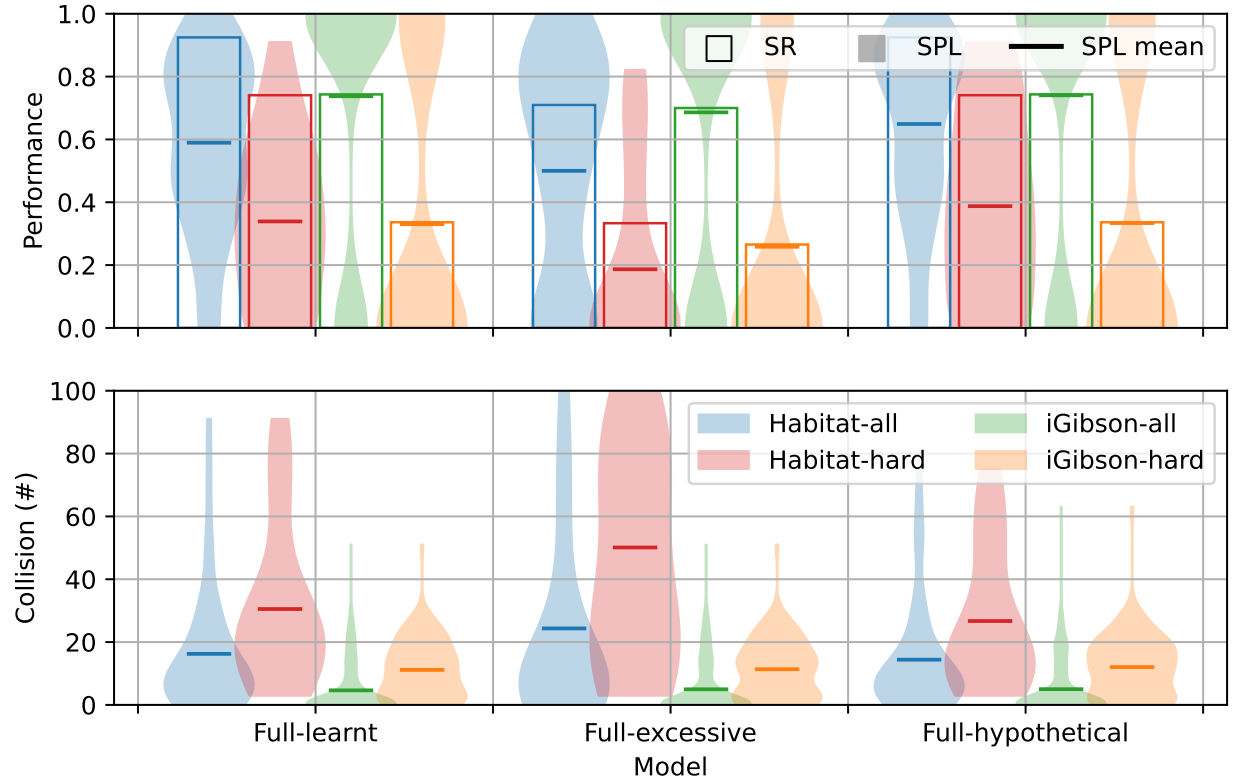


Figure 5: Performance of insect-inspired models with different memory consolidation mechanisms. Full-learnt: our insect-inspired model with selective memory consolidation. Full-excessive: the same model but with excessive, unconditional memory consolidation across all 20 trials. Full-hypothetical: a model memorising all trial experiences within an episode and cherrypicking the best performance.

(highest SPL) (Fig. 5). While it would be memory inefficient and thus impractical for both insects and robots to apply this brute-force method of saving all checkpoints, it prompts consideration of alternative memory consolidation mechanisms (to be discussed in §4.5.4).

3.4 Robust Control Using Reafference Only

Our model was finally validated in iGibson with imperfect motor control. In particular, the angular speed was constantly perturbed by artificial steering noise, $n_\omega \sim \text{Lognormal}(0, \sigma^2)$, and bias, $b_\omega \in (-1, 1)$, that is,

$$\omega_{\text{motor}} = \text{Clip}((\omega_{\text{model}} + b_\omega) \cdot n_\omega, -1, 1). \quad (8)$$

As the noise eliminated perfect determinism from our simulations, unlike in extensive testing in previous sections, we would not stop an episode immediately after a performance drop. Instead, an episode was always composed of 20 consecutive trials.

We emphasise that the model controlled the robot using visual reafferent inputs only. The perturbation by Equation (8) was unknown to the model, which received no efference copy by design. Even if the model could be potentially re-designed to process an efference copy, the artificial perturbation could still emulate imperfections in the robot's actuation and unknown factors in the environment. For comparison, the odometry-collision model was tested under identical conditions to the full model.

In the specific episode shown in Fig. 6, simulating a robot with severe intrinsic leftwards bias $b_\omega = 0.5$ and a mild noise $\sigma = 0.05$, the model learnt from its collision experience in a handful of the early trials, quickly finding a nearly optimal, mostly collision-free path. In contrast, without learning, the odometry-collision model always ran into the same obstacle(s) across all the trials.

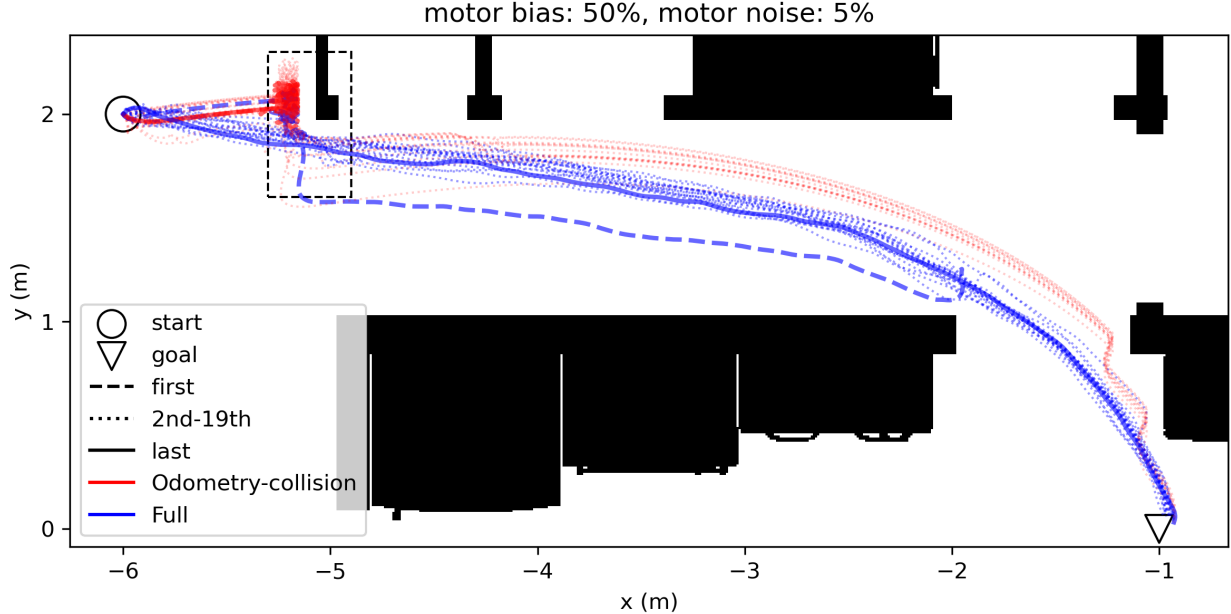


Figure 6: An example experiment with strong motor perturbation, $b_\omega = 0.5$ and $n_\omega = 0.05$. In 20 consecutive trials, the robot started at $(-6, 2)$ (circle) and the goal was to reach $(-1, 0)$ (triangle) with 500 frames. The circle denoting the start position is approximately the footprint of the robot. All the obstacles (black) are static. The trajectories in the area enclosed in the rectangle with dashed boundaries are depicted in more details in Supplementary Fig. 10.

To examine the robustness of the full model in more detail, using the same episode, we varied σ and b_ω separately (keeping the other at zero). We found the magnitude of the steering noise (for $\sigma \leq 1$) has little impact on the performance of the full and ablated models (Fig. 7). The full model almost always outperformed the ablated model in both metrics, except for $\sigma = 0.5$ when the full model yielded a lower SPL by approximately 0.1. Even within the earliest (5) trials, while the full model model was only slightly better in SPL, it accrued significantly less collisions than the ablated model, suggesting online learning even in the first trials is providing some benefit.

The steering bias manifested a greater effect (Fig. 8). The performance of the ablated model was largely dependent on the bias. The model could not reach the goal for $b_\omega \leq -0.3$, as the rightwards bias drove the robot too south onto the west-facing wall (from $(-5, 0)$ to $(-5, 1)$), preventing the robot from entering the west-to-east corridor. On the other

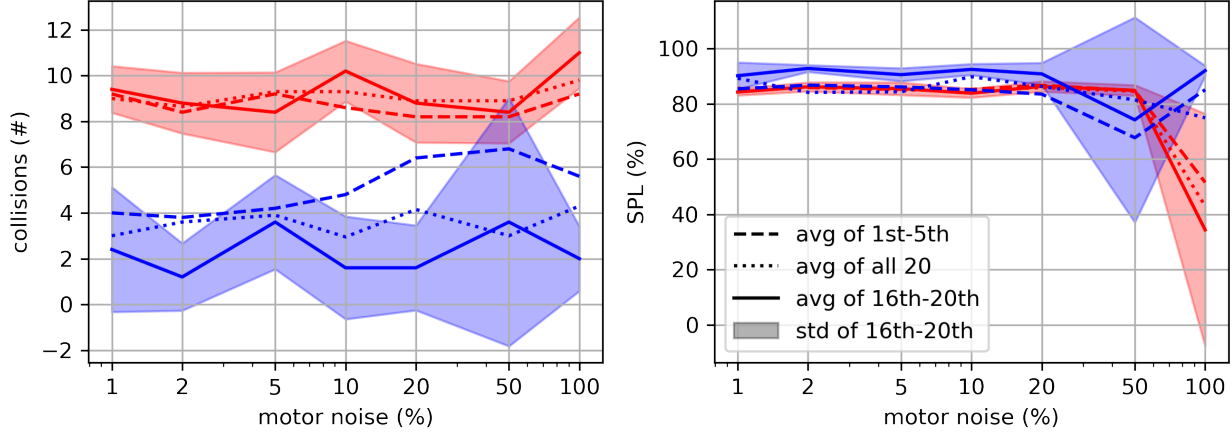


Figure 7: The effect of motor noise on performance. As before, blue is the full model and red the odometry-collision model. More details of trial-by-trial performance are shown in in Supplementary Fig. 11.

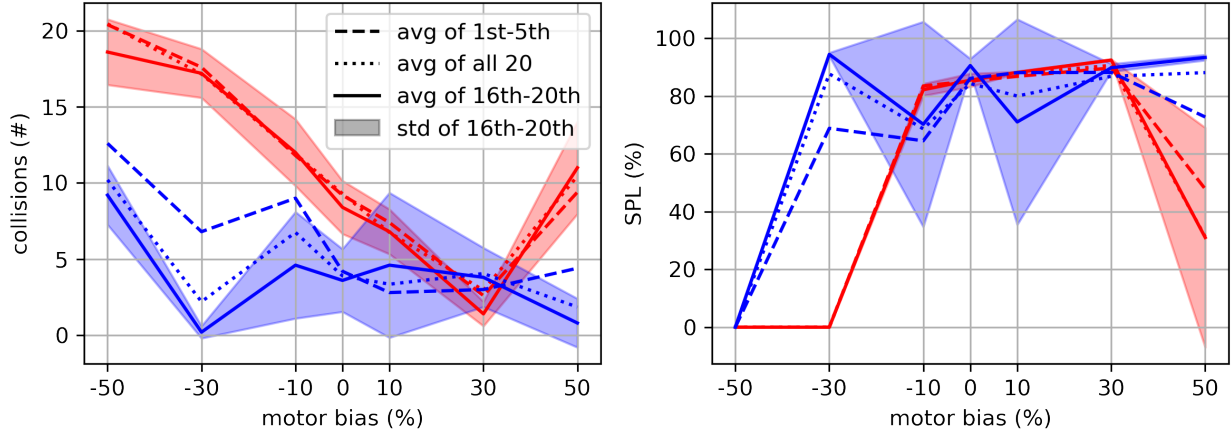


Figure 8: The effect of motor bias on performance. As before, blue is the full model and red the odometry-collision model. More details of trial-by-trial performance are shown in in Supplementary Fig. 12.

hand, the maximal performance was reached at $b_\omega = 0.3$, when paths were biased leftwards from the beeline into a shape coincidentally similar to the last path of the full model in Fig. 6.

In contrast, the full model was less affected by the bias. It could quickly learn to avoid obstacles and optimise paths, achieving on average an SPL of about 0.8 with less than 5 collisions. Although the full model could not overcome the largest rightwards bias ($b_\omega = -0.5$), failing to reach the goal due to the same obstacle (the west-facing wall) as the ablated model, (only) the full model could adapt to $b_\omega = -0.3$, avoiding the wall and reaching the goal.

The robustness against steering noise can be explained by the same observation from our previous work [27] (on route following) with the same robot in iGibson that most noise effects were smoothed out by the realistic, low-pass filtering motors during locomotion, while the control commands were generated by the model at relatively high frequency. Moreover, it is easier to mitigate steering bias in goal directed navigation, at least with our experiment setup, because the odometry data is accurate, preventing the model from catastrophic disorientation. As a result, even the odometry-collision agent could reach the goal with no learning and steering bias in some cases (Fig. 8).

4 Discussion

Ants can learn to negotiate cluttered environments while using path integration to relocate a target location such as their nest or a food source. In particular, after foraging and finding food, they attempt to return to their nest in a straight line, while quickly optimising their inbound paths with respect to obstacles [7]. This behaviour is formally equivalent to visual point-goal navigation, a popular benchmark in robotics. Here we develop a novel integrative model, based on two insect brain structures responsible for associative learning and PI, and evaluate it for controlling a robot during point-goal navigation in two different simulators, Habitat and iGibson. These simulators are similar in realistic visual rendering but differ in their underlying physics, resulting in two agents with drastically different action spaces (§2.2.3).

Previous models of the same learning circuit, the MB, have focused on associating views to positive progress made along a route, whereas the MB in our model learns only repulsive views, that is, the visual experience preceding an escape response from a collision. There is evidence for both forms of visual learning in insects, which we will discuss further below. Another difference from previous work is the introduction of selective memory consolidation, in the form of STM and LTM processes consistent with biological learning systems [41].

Moreover, our integrative model of the MB and the CX is distinct from previous ones [16, 17], which emulate successfully how insects navigate using learnt visual cues and PI but do not explain when and how learning occurs in the first place. Our model corroborates the hypothesis of [31] that an insect can ‘learn continuously the routes they travel’.

Compared to SOTA RL or SLAM solutions for this task, our system is extremely lightweight while still capable of comparable if not equivalent performance, with no pretraining. It combines mapless (local) motion planning with online learning in a minimal network with 64000 learnable parameters (more consistent with the brain size of ants and bees [50, 51], compared to the millions used in [46, 47]). The visual preprocessing is also much less expensive than the deep convolutional networks used in SLAM and RL approaches. Incurring minimal learning costs, it is computationally far more efficient, even without any optimisation effort.

4.1 Adaptive Obstacle Avoidance by Visual Learning

The MB of our model essentially performs the role of a visual compass by template matching [23], after learning the association between visual inputs and target directions. In terms of both architecture and function, it is almost identical to those in recent modelling and robotics works on insect-inspired visual route following [24, 37, 27] and homing [52, 37]. In particular, our model is mathematically equivalent to a model for visual homing or route following, if the direction to the goal is estimated from visual memory or always set to the agent’s own orientation (for any t , if $\theta(t) = \sigma(t)$, $\Delta\sigma(t) = \phi(t)$), respectively. However, learning in our model is only triggered just before collisions and after escapes, resulting in the MB memory formed primarily from repulsive views of obstacles, rather than attractive views acquired along a route or towards the goal in training.

As a result, our model learns visual obstacle avoidance on the fly. Note the underlying mechanism is conceptually more akin to the early work inspired by animals’ reflex reactions in general [38], rather than some recent insect-inspired work. [53] uses an MB circuit as a core decision-making module for their agent. However, the MB is integrated with other unsupervised learning and RL modules (for visual feature extraction and policy learning and selection, respectively), which also make significant contribution to successful visual obstacle avoidance according to the ablation study.

Compared to the homing and route following models that learn many views in training, the collision-triggered learning of our model entails fewer and less correlated views to be learnt by the MB. As the MB is functionally equivalent to a Bloom filter [40], learning fewer and less correlated views implies weaker interference in its memory and higher accuracy in obstacle recognition. Moreover, our model is prevented from excessive learning by performing selective memory consolidation that rejects memories damaging its navigation performance. Thus, it is relatively unlikely for our model to suffer from catastrophic disorientation, unless the scene is considerably cluttered, causing many collisions. In such cluttered scenes, however, instead of memory interference, the major concern would be whether the model could reach the goal.

4.2 Mapless Navigation by Goal Approaching and Obstacle Avoidance

To navigate towards a goal without a map or mapping, our model combines goal approaching and obstacle avoidance, a strategy adopted by many mapless navigation models, including insect-inspired ones [20, 21]. However, they consider predetermined (non-adaptive) obstacle avoidance only (similar to the odometry-collision model here), which does not allow for active optimisation of paths or to go around concave obstacles whereas these positive behavioural outcomes could emerge from learning (§3.2 and §3.4). We highlight that, as the (full) model kept learning on the fly, these positive

outcomes of learning (in comparison to the odometry-collision model) could be manifested even in its first attempt at an episode.

In terms of adaptive mapless navigation by collision-triggered learning and default goal approaching, the model is reminiscent of bug algorithms [54]. In particular, the ablated odometry-collision model resembles the simplest ‘common sense algorithm’ [55] that prioritises goal approaching unless encountering obstacles. In bug algorithms, it is assumed that boundaries of obstacles can be followed perfectly after collisions, and learning takes the form of explicitly and incrementally memorising an increasing number of collision coordinates. Neither of these occur in our model, and consequently, there is no guarantee (as promised by bug algorithms) that our agent would learn to avoid the collision positions or to reach a goal in an environment. However, as our model learns to recognise obstacles visually, it may generalise learnt obstacle avoidance to novel obstacles with similar appearances, whereas such generalisation is impossible in bug algorithms.

More crucially, in a realistic environment with odometry drifts and errors, bug algorithms are unable to uphold the theoretical guarantee of goal reaching [54]. In fact, as the magnitude of (simulated) odometry drifts increased, the simplest common sense algorithm which started out as the worst ends up the best amongst all the bug algorithms tested in [54]. In addition, [15] simulated a neural network model of the CX (with as few as 18 neurons) for odometry-based PI computation and demonstrated that it could robustly reach the goal (with the 0.2 m catchment, same as our success criterion) given sensory noise up to 2% (and that, even with 5% sensory noise, it yielded an average minimal distance to the goal under 0.4 m). While there were no obstacles in the simulations of [15] as in ours, they considered a much longer duration for a single trial, consisting of 10000 frames. Therefore, despite our model’s susceptibility to odometry and PI drifts and errors, we expect its performance to be more robust than most bug algorithms.

4.3 Learning with Sparse Reward

As the MB learning is modulated by reinforcement signals, our model is conceptually akin to RL, especially the VO+RL models [46, 47], for the decision-making process consisting of two steps, sensor-to-odometry and odometry-to-control. Moreover, [56, 57] consider the goal of the MB using reinforcement signals to be prediction error minimisation, leading to [58] further adopting the RL framework to explain insect navigation with hypothetical components of the MB.

The implementation details, however, distinct our model from these RL models. While learning is achieved by an ANN, the model (MB) uses the hetero-associative learning rule rather than backpropagation. The model does not try to minimise errors between its predictions and the true values of reinforcement signals via large amount of training, because the model relies on the strong prior of goal approaching and only makes adaptive adjustments after collisions, i.e., deviation from the direction to the goal for obstacle avoidance. In RL jargon, our model exploits a default, non-random ‘policy’ that yields mediocre performance and improves it via online learning.

Without such a default policy, an RL agent can rarely receive the actual success rewards in early stages of training, as it is almost impossible to reach a goal with a purely random policy [45, 1]. How to deal with such sparse rewards is a long-lasting challenge in RL in general, and one common solution, employed by the SOTA agents, is reward engineering, designing auxiliary, intermediate reinforcement signals that enable policy updating at a higher rate to accelerate RL. In particular, in addition to a large reward for reaching goal, the RL agents assumes a small reward for moving closer to the goal. Note ‘moving closer’ is reward-engineered in terms of the geodesic distance, rather than Euclidean distance, to the goal in all these works [1, 3, 46, 47], effectively leaking (part of) the information of the shortest paths to the goal to the RL agents before reaching it.

While this choice is permitted in the traditional machine learning paradigm that splits training and testing, it is incompatible with the online learning paradigm. Firstly, in a truly novel environment (with no prior mapping), accurate geodesic distances to the goal is always unknown. If the geodesic distance could somehow be estimated without a map, it would be trivial for an agent to treat the geodesic information as a potential field and then solve point-goal navigation by gradient ascent (or descent), e.g., chemotaxis, making training obsolete. Secondly, such auxiliary reinforcement must be set significantly small compared to the actual, sparse rewards. Otherwise, the agent would express more unexpected behaviours that effectively deprioritise the actual rewards, a phenomenon known as ‘rewarding hacking’ in the RL literature, or Goodhart’s law in wider contexts. As a result, large-scale, parallel training is a necessity for models to receive stable training signals [3], and there are always risks associated with the transferability across platforms and environments, e.g., abusing the sliding mechanism when colliding with obstacles [48].

In contrast, our model deals with the challenge of sparse rewards (of goal reaching) with the strong prior of goal approaching and the decomposition of its memory into different time scales. Selective memory consolidation guarantees that only learning benefitting overall performance (SPL) would be preserved in the long term. As minimal online learning (instead of large-scale training) suffices to yield great performance, our model is ready for deployment on any new platform in any novel environment.

4.4 Choice of Environment and Baseline

Although our model yielded ‘similar’ performance in both simulators (in terms of SR and SPL), the ablation study and the analysis on ‘hard’ episodes show that the performance, using the same metrics, was significantly dependent on simulators and episodes. In particular, our iGibson tasks were far easier than the Habitat ones, which might be rooted from differences in the low-level motion control, the particular indoor scenes, the objects contained in the scenes, or any other nuances. Similarly, [1] found model performance in Gibson 4+ scenes always better than that in Matterport3D, regardless of the training scenes in Gibson 4+ or Matterport3D scenes.

Indeed, all the Gibson scenes are probably designed to be easily navigable, as they are (primarily) civil facilities, ‘including households, offices, hotels, venues, museums, hospitals, construction sites’ [44], rather than prisons or military structures, which may be designed to challenge or restrict navigation. Such scenes may be particularly navigable to humans. With the only caveat that there was only *one* participant, [45] reports a human baseline with Matterport3D scenes, scoring SR = 0.953 and SPL = 0.867. Natural habitats of insects, especially to those capable of flying, are even more open than manmade facilities. The inherent traversability of the environments can largely explain the non-zero performance of the odometry-only models and the strong reliance on PI in insect navigation.

For any simulator or set of environments, it is useful to establish a ‘difficulty’ metric for different episodes (or equivalently an ‘environmental complexity’ measure). We suggest the performance of an odometry-only baseline might be more suitable metric than the current use of the ratio between the Euclidean and geodesic distances to the goal (termed ‘complexity’ in Habitat datasets) [1]. The odometry-only performance is straightforward to obtain and does not require full floor plans (for computing the geodesic distance). In addition, it is more behaviourally relevant. In the two hypothetical episodes depicted in Fig. 9, while Episode A is associated with a higher geodesic/Euclidian distance ratio due to the larger obstacle, the odometry-only agent would be able to solve Episode A but not Episode B, because the obstacle in Episode B is concave. Similarly, if the start and goal positions are swapped in either episode, the geodesic/Euclidian distance ratio would not change, but it is more difficult for an agent to get around a concave obstacle than a convex one. More generally, the difficulty of point-navigation task is fundamentally determined by all potential interactions between a robot and its environment, e.g., uncertainties in sensors and actuators, consequences of collisions (sliding or not), which are not reflected in the static floor plan of a scene, but can be accounted for by the odometry-only performance.

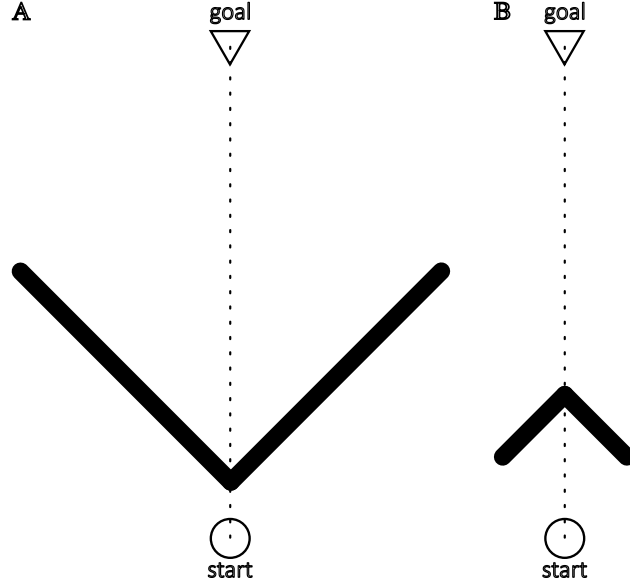


Figure 9: Two hypothetical point-goal navigation episodes. The (black) obstacles are symmetric in the beeline connecting the start and goal positions. From the agent’s perspective at the start, the obstacle is larger and convex in (A), but smaller and concave in (B).

4.5 Limitations and Future Work

4.5.1 Testing on Real Robots

The main limitation of this work is that our model was tested only in simulations, and, except when artificial noise was added, the physics, the visual rendering, and the odometry data were unrealistically deterministic and consistent within and across tests. While it is undoubtedly impressive that [2] managed to reach perfect performance in the Habitat task, the authors admitted in Appendix 8 that their analysis on model performance ‘*not* very indicative of the transfer performance to a real robot’. Indeed, [47] tested their best model (Model 4 in Table 2) in the real world without adaptation and found the SR dropped (from 0.96) to 0.11. Our model faces a similar, possibly serious, sim-to-real gap, because it also relies heavily on vision, and ambient lighting in the real world changes constantly. Nevertheless, the gap is expected to be smaller, because our model performs online learning in a time limited trial, during which the light should be at least more consistent than the transfer from offline training to testing.

4.5.2 Optimisation

In addition, our model has not been optimised in parameter choice or algorithmic implementation or for hardware. User-defined parameters, e.g., k , τ_e , α , and b_ω , were chosen arbitrarily without optimisation. As the PN-KC weights and the KC activity are sparse and binary, in principle, all computations in the MB can be further optimised for greater efficiency by executing addition (or subtraction) only. The visual preprocessing (§2.1.1) is obsolete, if a low-resolution, monochrome camera can be used instead.

4.5.3 Obstacle Detection and Depth Sensing

For better performance, the model might benefit from predictive obstacle detection replacing collision detection, probably based on depth sensing. Insects can estimate distances to objects by antennae and eyes, and robots by LiDAR and depth camera. On the same virtual robot in iGibson, our previous work [27] used depth data to reduce collisions, and performance gain in Habitat point-goal navigation was reported for all the models cited in §3 with RGBD inputs, compared to the same models but with RGB vision.

With depth sensing, the model can reduce the number of collisions. This will minimise the risk of physical damage to a real robot. Moreover, this will permit intrinsic obstacle avoidance, reducing the demand for learning and effectively improving efficiency and efficacy. Such an upgrade might benefit, in particular, navigation in an environment cluttered with obstacles or long-range navigation.

In addition, depth sensing will also allow the model to adopt proper obstacle boundary following as an escape strategy (as in bug algorithms, discussed in §4.2), which would guarantee the agent facing and learning a view of no obstacles after escape. It is expected to enhance locomotion and learning efficiency, as the current naive escape strategy may drive the robot into other obstacles.

4.5.4 Memory Consolidation and Continual Learning

Despite the performance benefits brought by the selective memory consolidation mechanism, it sometimes led the model performance (SPL) stuck in a local minima (§3.3). Indeed, the mechanism was inspired by memory traces at different time scales but configured to conveniently fit the temporal hierarchy of the Habitat task (consisting of consecutive trials that are identical in setup for each episode) without any theoretical insights or practical optimisation.

From the machine learning perspective, the online learning paradigm followed by our model can be formalised as a Markov Chain Monte Carlo process, implying the possibility of applying corresponding methods, e.g., Metropolis–Hastings algorithm, for memory consolidation (rejection). An alternatively, more biomimetic approach may consider the memory acquisition and consolidation process time (frame)-dependent, e.g., functionally following the temporal weighting rule as proposed by [29]. Moreover, such time-dependent mechanisms may also be more biologically realistic at the neural circuit level, in processing STM, ITM, and LTM, e.g., DPM modulation [41], multi-MBON encoding [42], homeostatic regulation [59].

Moreover, it is possible and perhaps desired to integrate the classical machine learning (RL) paradigm with excessive training and the online learning paradigm, so that an agent can exploit prior experience for navigation in a new environment and adapt rapidly to any novel characteristics. The human baseline mentioned earlier in §4.4 followed this hybrid paradigm, as the participant was tested directly in the novel (virtual) scenes [45] and presumably, as a human, they had experienced many similar scenes in their life.

The hybrid paradigm can be formalised as *continual learning*, which is generally considered more challenging, ultimately because the environment may generate data streams that, by their nature, are dynamic, rather than statistically

stable. In particular for navigation, there is no guarantee in similarities between training and testing scenes. For exactly the same reasons, continual learning is useful because most natural environments are dynamic. In practice, the major practical challenge for agents, especially those using neural networks for learning, e.g., the RL models, is known as catastrophic forgetting [60] (or the stability-plasticity dilemma [61]), which entails the high risk of new memories eroding or even erasing old ones during learning.

As our model performs online learning from scratch, it encounters the same challenge of continual learning from the opposite angle. Instead of worrying the LTM memory being forgotten, our approach demands deeper understanding on what and how LTM should be preserved, in order to extend the model for greater transferability across scenes. A workable solution to the ‘how’ question is somewhat available from [62], in which an MB model, similar to ours in architecture, was demonstrated capable of continual learning. However, the model was tested in a visual classification task with well-defined labels (for the MBONs), which is not directly applicable in goal-directed navigation, as the answer to the ‘what’ question is ultimately determined by the long-term interactions between an agent and its environment.

4.5.5 Visual Homing and Long-range Navigation

As mentioned in §4.2 and §4.5, drifting errors in odometry and PI and changes in ambient lighting are expected to be the most detrimental factors. It would be particularly crucial to mitigate them in long-range or duration navigation. Insects rely strongly but not only on PI for navigation. They are capable of homing even after being caught and released at a different position (if not too far away from their nests), perhaps leveraging visual or other sensory cues [63, 64]. Similarly, our model can be extended for more robust navigation while remaining mapless and lightweight.

In particular, our model and the previous MB-CX models [16], capable of switching between visual homing and route following, can be integrated, so that the extended model would also benefit from learnt visual obstacle avoidance, and its learning would occur spontaneously as needed in testing. The models, in particular their MBs, are immediately ready to be merged by extending the MB with extra MBONs, as the architectures are almost identical, all inspired from real insect MBs. Indeed, it is more consistent with the real MB to have separate MBONs for learning attractive and repulsive stimuli [65]. In particular, the homing behaviour is more robust with different MBONs learning views towards the goal and those in the opposite direction [66]. Functionally, this extension will result in an adaptive, visual potential field as used in local path planning, which is expected to be practically useful, considering the noise robustness in odometry-only goal-directed navigation demonstrated by the simulations of [15] and the commendable visual route following and homing performance of the real robot of [37]. To balance exploration and exploitation, the agent should prioritise repulsive memories first and eventually rely more on attractive memories.

Given the efficacy of visual homing [52, 37, 67], it is in principle viable to further mitigate drifting errors by scaling up the model with more MBONs, each responsible for learning and recognising views near different positions, effectively making the model SLAM-like.

4.5.6 Multi-agent System

The efficient computing and the lightweight architecture of our model suggest good potential of scaling up into a multi-agent system in simulations or the real world. In a more naturalistic environment, from the perspective of a swarm of insects or robots, there are potentially multiple goals, and the performance of individuals is outweighed by that of the swarm. Consequently, having capabilities of coordination and communication in addition to imperfect navigation skills might be more important than perfecting individual navigation with a diminishing improvement at an exponentially growing cost.

References

- [1] Manolis Savva, Abhishek Kadian, Oleksandr Maksymets, Yili Zhao, Erik Wijmans, Bhavana Jain, Julian Straub, Jia Liu, Vladlen Koltun, Jitendra Malik, et al. Habitat: a platform for embodied AI research. In *Proceedings of the IEEE/CVF international conference on computer vision*, pages 9339–9347, 2019.
- [2] Santhosh K Ramakrishnan, Aaron Gokaslan, Erik Wijmans, Oleksandr Maksymets, Alex Clegg, John Turner, Eric Undersander, Wojciech Galuba, Andrew Westbury, Angel X Chang, et al. Habitat-Matterport 3D dataset (HM3D): 1000 large-scale 3D environments for embodied AI. *arXiv preprint arXiv:2109.08238*, 2021.
- [3] Erik Wijmans, Abhishek Kadian, Ari Morcos, Stefan Lee, Irfan Essa, Devi Parikh, Manolis Savva, and Dhruv Batra. DD-PPO: learning near-perfect pointgoal navigators from 2.5 billion frames. *arXiv preprint arXiv:1911.00357*, 2019.
- [4] Martin Müller and Rüdiger Wehner. Path integration in desert ants, *Cataglyphis fortis*. *Proceedings of the National Academy of Sciences*, 85(14):5287–5290, 1988.

- [5] Thomas S Collett, Elisabeth Dillmann, A Giger, and Rüdiger Wehner. Visual landmarks and route following in desert ants. *Journal of Comparative Physiology A*, 170:435–442, 1992.
- [6] Antoine Wystrach, Sebastian Schwarz, Patrick Schultheiss, Guy Beugnon, and Ken Cheng. Views, landmarks, and routes: how do desert ants negotiate an obstacle course? *Journal of Comparative Physiology A*, 197:167–179, 2011.
- [7] Cody A Freas and Ken Cheng. Visual learning, route formation and the choreography of looking back in desert ants, *Melophorus bagoti*. *Animal Behaviour*, 222:123125, 2025.
- [8] Yoshinori Aso, Daisuke Hattori, Yang Yu, Rebecca M Johnston, Nirmala A Iyer, Teri-TB Ngo, Heather Dionne, LF Abbott, Richard Axel, Hiromu Tanimoto, et al. The neuronal architecture of the mushroom body provides a logic for associative learning. *eLife*, 3:e04577, 2014.
- [9] Barbara Webb. Beyond prediction error: 25 years of modeling the associations formed in the insect mushroom body. *Learning & Memory*, 31(5):a053824, 2024.
- [10] Daisuke Hattori, Yoshinori Aso, Kurtis J Swartz, Gerald M Rubin, L F Abbott, and Richard Axel. Representations of novelty and familiarity in a mushroom body compartment. *Cell*, 169(5):956–969, 2017.
- [11] Thomas Stone, Barbara Webb, Andrea Adden, Nicolai Ben Weddig, Anna Honkanen, Rachel Templin, William Wcislo, Luca Scimeca, Eric Warrant, and Stanley Heinze. An anatomically constrained model for path integration in the bee brain. *Current Biology*, 27(20):3069–3085, 2017.
- [12] Barbara Webb. The internal maps of insects. *Journal of Experimental Biology*, 222(Suppl_1):jeb188094, 2019.
- [13] Brad K Hulse, Hannah Haberkern, Romain Franconville, Daniel Turner-Evans, Shin-ya Takemura, Tanya Wolff, Marcella Noorman, Marisa Dreher, Chuntao Dan, Ruchi Parekh, et al. A connectome of the *Drosophila* central complex reveals network motifs suitable for flexible navigation and context-dependent action selection. *eLife*, 10, 2021.
- [14] Florent Le Moël, Thomas Stone, Mathieu Lihoreau, Antoine Wystrach, and Barbara Webb. The central complex as a potential substrate for vector based navigation. *Frontiers in Psychology*, 10:690, 2019.
- [15] Dennis Goldschmidt, Poramate Manoonpong, and Sakyasingha Dasgupta. A neurocomputational model of goal-directed navigation in insect-inspired artificial agents. *Frontiers in Neurorobotics*, 11:20, 2017.
- [16] Xuelong Sun, Shigang Yue, and Michael Mangan. A decentralised neural model explaining optimal integration of navigational strategies in insects. *eLife*, 9:e54026, 2020.
- [17] Roman Goulard, Stanley Heinze, and Barbara Webb. Emergent spatial goals in an integrative model of the insect central complex. *PLOS Computational Biology*, 19(12):e1011480, 2023.
- [18] Antoine Wystrach. Neurons from pre-motor areas to the mushroom bodies can orchestrate latent visual learning in navigating insects. *bioRxiv*, 2023.
- [19] Jan Stankiewicz and Barbara Webb. Using the neural circuit of the insect central complex for path integration on a micro aerial vehicle. In *Conference on Biomimetic and Biohybrid Systems*, pages 325–337. Springer, 2020.
- [20] Bart Baddeley, Paul Graham, Philip Husbands, and Andrew Philippides. A model of ant route navigation driven by scene familiarity. *PLOS Computational Biology*, 8(1):e1002336, 2012.
- [21] Xuelong Sun, Qinbing Fu, Jigen Peng, and Shigang Yue. An insect-inspired model facilitating autonomous navigation by incorporating goal approaching and collision avoidance. *Neural Networks*, 165:106–118, 2023.
- [22] Andrew Philippides, Bart Baddeley, Ken Cheng, and Paul Graham. How might ants use panoramic views for route navigation? *Journal of Experimental Biology*, 214(3):445–451, 2011.
- [23] Frédéric Labrosse. The visual compass: Performance and limitations of an appearance-based method. *Journal of Field Robotics*, 23(10):913–941, 2006.
- [24] Paul Ardin, Fei Peng, Michael Mangan, Konstantinos Lagogiannis, and Barbara Webb. Using an insect mushroom body circuit to encode route memory in complex natural environments. *PLOS Computational Biology*, 12(2):e1004683, 2016.
- [25] Aleksandar Kodzhabashev and Michael Mangan. Route following without scanning. In Stuart P. Wilson, Paul F.M.J. Verschure, Anna Mura, and Tony J. Prescott, editors, *Biomimetic and Biohybrid Systems.*, pages 199–210, Cham, 2015. Springer International Publishing.
- [26] Fabian Steinbeck, Efstathios Kagioulis, Alex Dewar, Andrew Philippides, Thomas Nowotny, and Paul Graham. Familiarity-taxis: a bilateral approach to view-based snapshot navigation. *Adaptive Behavior*, 32(5):407–420, October 2024.

[27] Yihe Lu, Jiahao Cen, Rana Maroun Alkhoury, and Barbara Webb. Insect-inspired embodied visual route following. *Journal of Bionic Engineering*, 2025.

[28] Ralf Möller. Insect visual homing strategies in a robot with analog processing. *Biological Cybernetics*, 83(3):231–243, 2000.

[29] Cody A Freas and Ken Cheng. Learning and time-dependent cue choice in the desert ant, *Melophorus bagoti*. *Ethology*, 123(8):503–515, 2017.

[30] Cody A Freas and Marcia L Sprecher. Terrestrial cue learning and retention during the outbound and inbound foraging trip in the desert ant, *cataglyphis velox*. *Journal of Comparative Physiology A*, 205(2):177–189, 2019.

[31] Leo Clement, Sebastian Schwarz, and Antoine Wystrach. Latent learning without map-like representation of space in navigating ants. *bioRxiv*, pages 2024–08, 2024.

[32] Chengshu Li, Fei Xia, Roberto Martín-Martín, Michael Lingelbach, Sanjana Srivastava, Bokui Shen, Kent Elliott Vainio, Cem Gokmen, Gokul Dharan, Tanish Jain, Andrey Kurenkov, Karen Liu, Hyowon Gweon, Jiajun Wu, Li Fei-Fei, and Silvio Savarese. iGibson 2.0: object-centric simulation for robot learning of everyday household tasks. In *Proceedings of the 5th Conference on Robot Learning*, volume 164 of *Proceedings of Machine Learning Research*, pages 455–465. PMLR, 08–11 Nov 2022.

[33] David Marr and Ellen Hildreth. Theory of edge detection. *Proceedings of the Royal Society of London. Series B. Biological Sciences*, 207(1167):187–217, 1980.

[34] Sebastian Schwarz, Ajay Narendra, and Jochen Zeil. The properties of the visual system in the Australian desert ant *Melophorus bagoti*. *Arthropod Structure & Development*, 40(2):128–134, 2011.

[35] H Sebastian Seung. Predicting visual function by interpreting a neuronal wiring diagram. *Nature*, 634(8032):113–123, 2024.

[36] Antoine Wystrach, Alex Dewar, Andrew Philippides, and Paul Graham. How do field of view and resolution affect the information content of panoramic scenes for visual navigation? A computational investigation. *Journal of Comparative Physiology A*, 202:87–95, 2016.

[37] Gabriel G Gattaux, Antoine Wystrach, Julien R Serres, and Franck Ruffier. Route-centric ant-inspired memories enable panoramic route-following in a car-like robot. *Nature Communications*, 16(1):8328, 2025.

[38] Bernd Porr and Florentin Wörgötter. Isotropic-sequence-order learning in a closed-loop behavioural system. *Philosophical Transactions of the Royal Society of London. Series A: Mathematical, Physical and Engineering Sciences*, 361(1811):2225–2244, 2003.

[39] Johannes Felsenberg, Pedro F Jacob, Thomas Walker, Oliver Barnstedt, Amelia J Edmondson-Stait, Markus W Pleijzier, Nils Otto, Philipp Schlegel, Nadiya Sharifi, Emmanuel Perisse, et al. Integration of parallel opposing memories underlies memory extinction. *Cell*, 175(3):709–722, 2018.

[40] Sanjoy Dasgupta, Timothy C Sheehan, Charles F Stevens, and Saket Navlakha. A neural data structure for novelty detection. *Proceedings of the National Academy of Sciences*, 115(51):13093–13098, 2018.

[41] Ronald L Davis. Traces of drosophila memory. *Neuron*, 70(1):8–19, 2011.

[42] Evripidis Gkantas, Li Yan McCurdy, Michael N Nitabach, and Barbara Webb. An incentive circuit for memory dynamics in the mushroom body of *Drosophila melanogaster*. *eLife*, 11:e75611, 2022.

[43] Bokui Shen, Fei Xia, Chengshu Li, Roberto Martín-Martín, Linxi Fan, Guanzhi Wang, Claudia Pérez-D'Arpino, Shyamal Buch, Sanjana Srivastava, Lyne Tchapmi, et al. iGibson 1.0: a simulation environment for interactive tasks in large realistic scenes. In *2021 IEEE/RSJ International Conference on Intelligent Robots and Systems (IROS)*, pages 7520–7527. IEEE, 2021.

[44] Fei Xia, Amir R. Zamir, Zhi-Yang He, Alexander Sax, Jitendra Malik, and Silvio Savarese. Gibson Env: real-world perception for embodied agents. In *Computer Vision and Pattern Recognition (CVPR), 2018 IEEE Conference on*. IEEE, 2018.

[45] Dmytro Mishkin, Alexey Dosovitskiy, and Vladlen Koltun. Benchmarking classic and learned navigation in complex 3D environments. *arXiv preprint arXiv:1901.10915*, 2019.

[46] Xiaoming Zhao, Harsh Agrawal, Dhruv Batra, and Alexander Schwing. The surprising effectiveness of visual odometry techniques for embodied pointgoal navigation. In *2021 IEEE/CVF International Conference on Computer Vision (ICCV)*, pages 16107–16116, 2021.

[47] Ruslan Partsey, Erik Wijmans, Naoki Yokoyama, Oles Dobosevych, Dhruv Batra, and Oleksandr Maksymets. Is mapping necessary for realistic pointgoal navigation? In *2022 IEEE/CVF Conference on Computer Vision and Pattern Recognition (CVPR)*, pages 17211–17220, 2022.

[48] Abhishek Kadian, Joanne Truong, Aaron Gokaslan, Alexander Clegg, Erik Wijmans, Stefan Lee, Manolis Savva, Sonia Chernova, and Dhruv Batra. Sim2real predictivity: does evaluation in simulation predict real-world performance? *IEEE Robotics and Automation Letters*, 5(4):6670–6677, 2020.

[49] Manolis Savva, Angel X. Chang, Alexey Dosovitskiy, Thomas Funkhouser, and Vladlen Koltun. MINOS: multimodal indoor simulator for navigation in complex environments. *arXiv:1712.03931*, 2017.

[50] Randolph Menzel and Martin Giurfa. Cognitive architecture of a mini-brain: the honeybee. *Trends in Cognitive Sciences*, 5(2):62–71, 2001.

[51] R Keating Godfrey, Mira Swartzlander, and Wulfila Gronenberg. Allometric analysis of brain cell number in Hymenoptera suggests ant brains diverge from general trends. *Proceedings of the Royal Society B*, 288(1947):20210199, 2021.

[52] Antoine Wystrach, Florent Le Moël, Leo Clement, and Sebastian Schwarz. A lateralised design for the interaction of visual memories and heading representations in navigating ants. *bioRxiv*, 2020.

[53] Liying Tao, Zonglin Yang, Gaoming Li, and Delong Shang. Obstacle avoidance in a crowd with a plastic recurrent mushroom body model. *IEEE Access*, 2025.

[54] Kimberly N McGuire, Guido C H E de Croon, and Karl Tuyls. A comparative study of bug algorithms for robot navigation. *Robotics and Autonomous Systems*, 121:103261, 2019.

[55] V. Lumelsky and A. Stepanov. Dynamic path planning for a mobile automaton with limited information on the environment. *IEEE Transactions on Automatic Control*, 31(11):1058–1063, 1986.

[56] James EM Bennett, Andrew Philippides, and Thomas Nowotny. Learning with reinforcement prediction errors in a model of the *Drosophila* mushroom body. *Nature Communications*, 12(1):2569, 2021.

[57] Anna-Maria Jürgensen, Panagiotis Sakagiannis, Michael Schleyer, Bertram Gerber, and Martin Paul Nawrot. Prediction error drives associative learning and conditioned behavior in a spiking model of *Drosophila* larva. *iScience*, 27(1), 2024.

[58] Stephan Lochner, Daniel Honerkamp, Abhinav Valada, and Andrew D Straw. Reinforcement learning as a robotics-inspired framework for insect navigation: from spatial representations to neural implementation. *Frontiers in Computational Neuroscience*, 18:1460006, 2024.

[59] Jacqueline T Weiss and Jeffrey M Donlea. Sleep deprivation results in diverse patterns of synaptic scaling across the *Drosophila* mushroom bodies. *Current Biology*, 31(15):3248–3261, 2021.

[60] Robert M French. Catastrophic forgetting in connectionist networks. *Trends in Cognitive Sciences*, 3(4):128–135, 1999.

[61] Stephen Grossberg. Processing of expected and unexpected events during conditioning and attention: a psychophysiological theory. *Psychological Review*, 89(5):529, 1982.

[62] Yang Shen, Sanjoy Dasgupta, and Saket Navlakha. Reducing catastrophic forgetting with associative learning: a lesson from fruit flies. *Neural Computation*, 35(11):1797–1819, 2023.

[63] Mario Pahl, Hong Zhu, Jürgen Tautz, and Shaowu Zhang. Large scale homing in honeybees. *PLOS One*, 6(5):e19669, 2011.

[64] Antoine Wystrach, Guy Beugnon, and Ken Cheng. Ants might use different view-matching strategies on and off the route. *Journal of Experimental Biology*, 215(1):44–55, 2012.

[65] Yoshinori Aso, Divya Sitaraman, Toshiharu Ichinose, Karla R Kaun, Katrin Vogt, Ghislain Belliart-Guérin, Pierre-Yves Plaçais, Alice A Robie, Nobuhiro Yamagata, Christopher Schnaitmann, et al. Mushroom body output neurons encode valence and guide memory-based action selection in drosophila. *eLife*, 3:e04580, 2014.

[66] Florent Le Moël and Antoine Wystrach. Opponent processes in visual memories: A model of attraction and repulsion in navigating insects’ mushroom bodies. *PLOS Computational Biology*, 16(2):e1007631, 2020.

[67] Xiaoting Zhong, Xuelong Sun, and Haiyang Li. A comparative study of reinforcement learning and insect-inspired visual navigation methods. In *Conference on Biomimetic and Biohybrid Systems*, pages 163–175. Springer, 2025.

5 Appendix

5.1 Model Details

See Table 3.

Table 3: More details of the recent point-goal navigation models in Table 2. Only [1] reports performance of both RL and SLAM models. In the Reward column, ++ denotes a large (positive) reward at the end of a training trial (if succeeded), and - a small punishment at every frame of the trial.

Reference	Training Scenes	RL/SLAM Method	Reward	Vision
[45]	SunCG, Matterport3D	ORB-SLAM2, D* Lite	—	CNN
[1]	Gibson 4+, Matterport3D	PPO/inherited from [45]	SR++, geodesic-, frame-	CNN
[3]	Gibson 2+, Matterport3D	DDPPO	SPL++, geodesic-, frame-	SE-ResNeXt50
[46]	Gibson 4+	inherited from [3]	inherited from [3]	ResNet18
[47]	Gibson 0+	inherited from [3]	inherited from [3]	ResNet50
[2]	HM3D	inherited from [3]	inherited from [3]	ResNet50

5.2 Supplementary Figures

See Fig. 10-12.

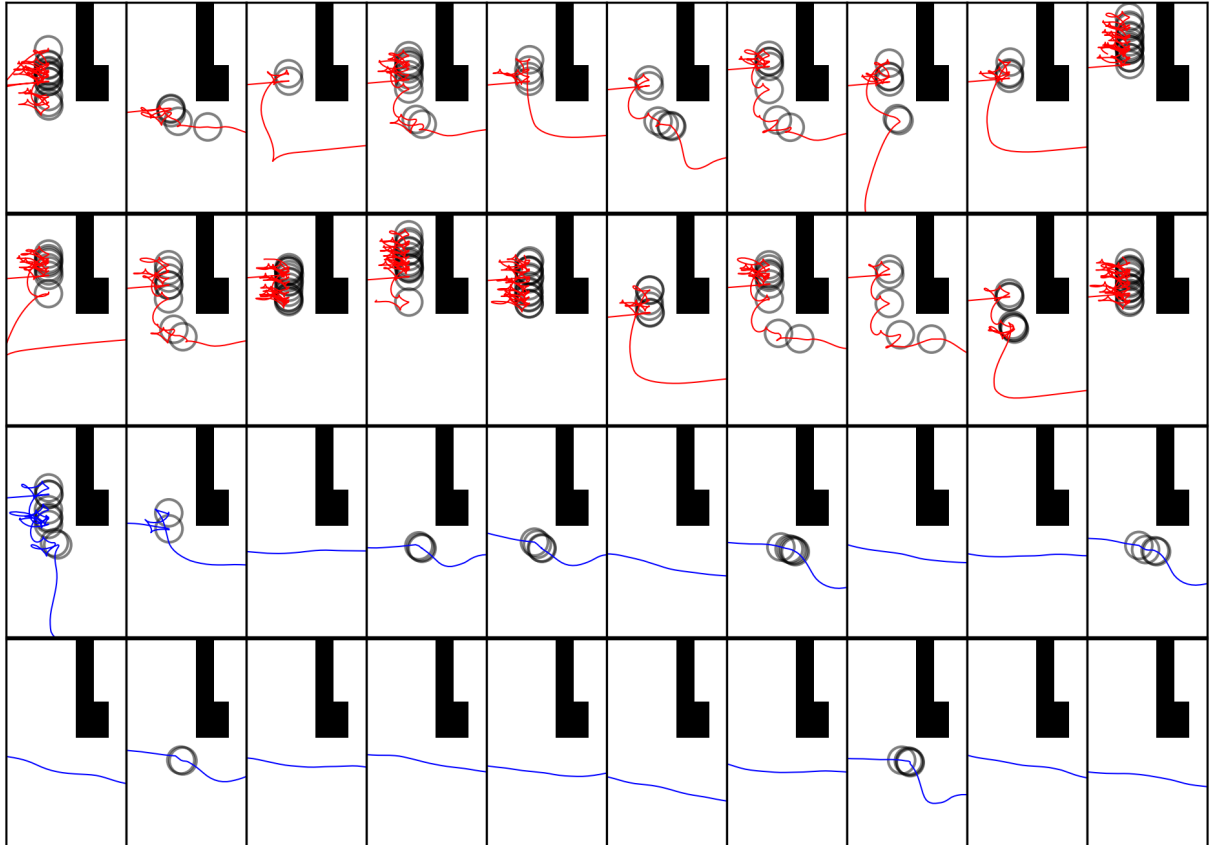


Figure 10: Zoom-in plots of the area enclosed in the rectangle with dashed boundaries in Fig. 6. The black circles here denote where collisions were detected.

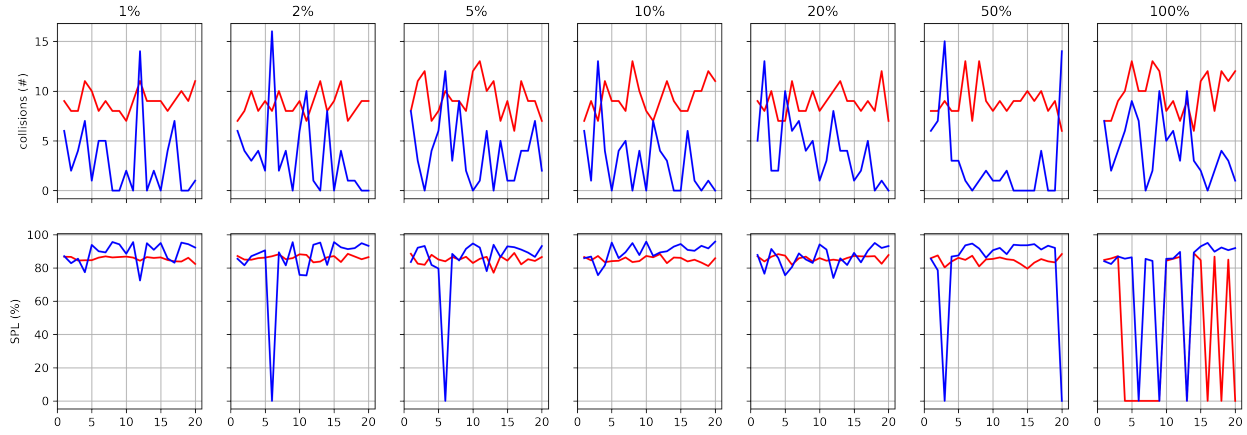


Figure 11: The effect of motor noise on performance, across trials within an episode. Blue is the full model, red is ablated (odometry-collision).

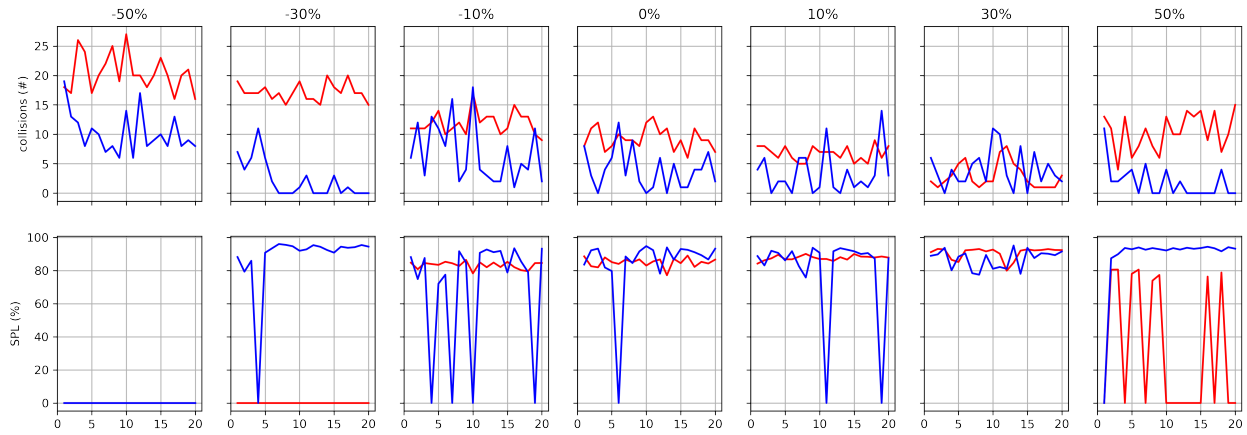


Figure 12: The effect of motor bias on performance, across trials within an episode. Blue is the full model, red is ablated (odometry-collision).